THEORETICAL NOTES

NOTE 365

NOVEMBER 1995

DISTRIBUTION FUNCTIONS OF THE HEMP ENVIRONMENT

K.-D. Leuthäuser

Fraunhofer-Institut für Naturwissenschaftlich-Technische Trendanalysen
P.O.B. 14 91, 53864 Euskirchen, Germany

ABSTRACT

The EXEMP code (Theoretical Note No. 363) is employed to evaluate cumulative distribution functions and mean values of characteristic pulse parameters over the HEMP ground coverage area, e.g. peak electric field, peak rate of rise, energy fluence, impulse, and polarization. The influences of yield and height of burst are also considered. Bivariate cumulative distribution functions and the corresponding probability densities linking any two of the above parameters are investigated to derive HEMP environments less stringent than worst case.

1. Introduction

A complete threat environment generated by high-altitude nuclear bursts requires the knowledge of the variation of the various threat parameters (e.g. peak electric field, peak rate of rise, energy fluence, polarization) over the total ground coverage area. This is particularly desirable whenever a more refined specification of the environment is needed for EMP interaction problems than solely by means of a worst case waveform.

The EXEMP code [1,2] developed by the author is particularly well suited to meet these requirements. It allows not only for variation of the observer location with respect to Ground Zero but also for parametric modifications of height of burst, nuclear weapon yield and earth magnetic field.

The present paper focusses on distributions of the various EMP waveform parameters. Having the well-known "smile-face" contour plots of the peak electric field in mind, this could be the portion of the total coverage area A_T for which the electric field E exceeds (or falls below) a certain field strength E_o. On the other hand, if the ground observer is considered to be uniformly distributed within the total coverage area (i.e. all locations are of equal value), the respective area portions can also be interpreted as cumulative distribution or probability functions $Pr(E > E_o)$ when normalized by the total area A_T. Bivariate probability functions, e.g. with respect to peak electric field and peak rate of rise, will also be discussed. Such functions might be useful if it is intended to specify more relieved threat levels than worst case.

2. EMP Coverage Areas and Cumulative Distribution Functions

In order to reduce the information provided by the exact time dependency of the whole variety of calculated waveforms, they can be typified by the following characteristic parameters [2]

1. peak electric field $Q_1 \equiv E_{pk}$ (1)

2. peak rate of rise $Q_2 \equiv (dE/dt)_{pk}$ (2)

3. energy fluence $Q_3 \equiv W_\infty = \frac{1}{Z_o} \int_{-\infty}^{+\infty} E^2(t)\, dt$ (3)

4. "impulse" $Q_4 \equiv I_\infty = \int_{-\infty}^{+\infty} E(t)\, dt.$ (4)

Sometimes, rise time T_r and half-width $T_{½}$ of the pulse are also specified. Adopting an analytical expression for the waveform E(t), e.g. the quotient of the sum of two exponentials (QEXP) or the difference of two exponentials (DEXP), T_r and $T_{½}$ can be estimated from the characteristic quantities Q_i [2,3].

To complete the HEMP environment the polarization of the incident plane wave will also be considered [4,5].

Having calculated Q_i (i = 1,....,4) and the polarization parameters for a sufficiently large number of different observer locations within the total coverage area, the relative portion of the total coverage area A_T for which Q is greater than a fixed value Q_o can be evaluated by numerical integration

$$Pr(Q > Q_o) = \frac{A(Q > Q_o)}{A_T} = \frac{1}{A_T} \int_{-\pi}^{+\pi} d\phi \int_0^{R_T} dR \sin\frac{R}{R_E}\, u(Q(R,\phi) - Q_o) \quad (5)$$

where R_E = 6370 km is the earth radius, R, ϕ are polar coordinates on the curved earth surface with the origin at Ground Zero (in the EXEMP code $\phi = 0°$ and 90° correspond to eastern and northern directions, respectively) and u(Q) is the Heaviside step function.

Furthermore, for H_o as the height of burst, the tangent radius is given by

$$R_T = R_E \arccos\frac{R_E}{R_E + H_o} \quad (6)$$

and the total coverage area

$$A_T = \int_{-\pi}^{+\pi} d\phi \int_0^{R_T} dR \sin\frac{R}{R_E} = 2\pi\frac{H_o R_E^2}{R_E + H_o} . \qquad (7)$$

Eq.(5) is evaluated by a Monte Carlo calculation. To proceed, Eq. (7) is rewritten as

$$A_T = 2\pi R_E^2 \left(1-\cos\frac{R_T}{R_E}\right) \int_0^1 dx \int_0^1 dy \qquad (8)$$

where
$$x = \frac{\cos\frac{R}{R_E} - \cos\frac{R_T}{R_E}}{1-\cos\frac{R_T}{R_E}} \qquad (9a)$$

and
$$y = \frac{\phi}{2\pi}. \qquad (9b)$$

Hence, a quasi-uniform distribution of random observer locations over the curved coverage area is obtained with the coordinates

$$\phi = 2\pi y \qquad (10a)$$

$$R = \arccos\left((1-x)\cos\frac{R_T}{R_E} + x\right) \qquad (10b)$$

where x and y are now random numbers unifomly distributed between 0 and 1. $\Pr\left(Q > Q_o\right)$ is then simply given by the number of observed random variables with $Q\left(R(x), \phi(y)\right) > Q_o$ divided by the total sample size N.

The sample of random variables $Q_i\left(R(x), \phi(y)\right)$ $(i = 1,...,4)$ was then computed using the EXEMP Code. As input, a QEXP shape monoenergetic (2 MeV) gamma source function with a Rossi-α of $2\,ns^{-1}$ and a decay constant β of $0.1\,ns^{-1}$ was chosen. The total gamma yield was 10 kt except for a few cases with varying gamma yield (Figs. 5 and 6). All calculations refer to an earth magnetic latitude of 50°.

Figures 1 to 4 show the portion of the coverage areas $A\left(Q_i > Q_{i,o}\right)$ as a function of height of burst with $Q_{i,o}$ as curve parameters. The dashed curve

denotes the limiting values $A(Q_i > 0) = A_T$ as given by Eq. (7). Although $Q_{i,o}$ can become arbitrarily small at the "blind spot" at $R \cong 0.4\ H_o$ northward of Ground Zero ($\phi = 90°$), the envelope is in general approximately determined already by $A(Q_i > Q_i(R_T))$ because the portion of the "blind spot" area becomes comparably small. The latter could have been better resolved by calculating

$$A\left(Q_i < Q_{i,o}\right) = A_T - A\left(Q_i > Q_{i,o}\right) \tag{11}$$

in a logarithmic scale.

The maximum and average values of Q_i are summarized in Table 1. The heights of burst for which the different Q_i acquire their respective maxima are (see also [2])

$E_{pk} = 65\ kV/m$ at $H_o = 120\ km$

$(dE/dt)_{pk} = 42\ kV/m/ns$ at $H_o = 80\ km$

$W_\infty = 0.10\ J/m^2$ at $H_o = 230\ km$

$I_\infty = 2.05 \times 10^{-3}\ Vs/m$ at $H_o = 600\ km$

Modifications of the maxima would have to be anticipated for a Rossi-α different from $2\ ns^{-1}$, in particular for the peak rate of rise and the peak electric field, and for gamma yields different from 10 kt.

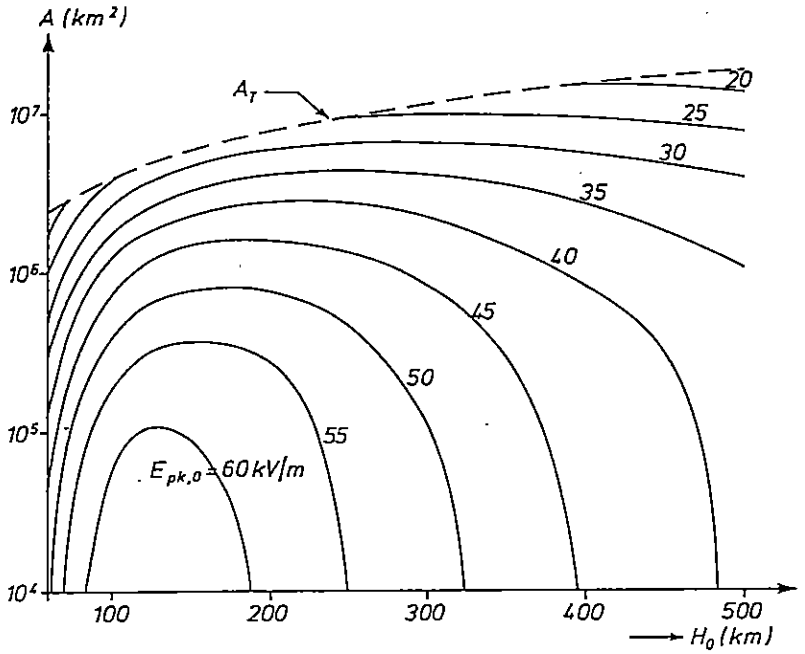

Fig. 1 Partial coverage area $A = A(E_{pk} > E_{pk,o})$ as a function of height of burst (A_T: total coverage area, $Y_\gamma = 10$ kt).

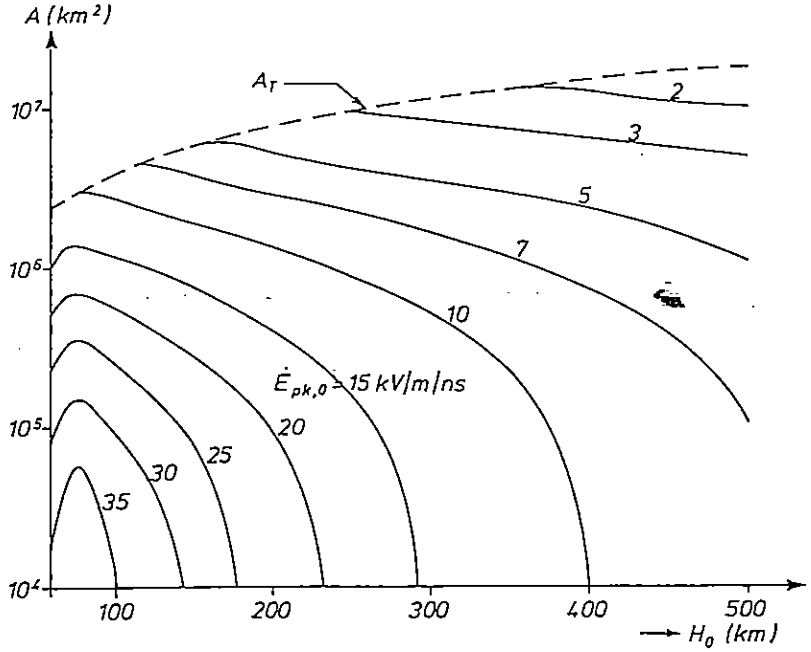

Fig. 2 Partial coverage area $A = A(\dot{E}_{pk} > \dot{E}_{pk,o})$ as a function of height of burst (A_T: total coverage area, $Y_\gamma = 10$ kt).

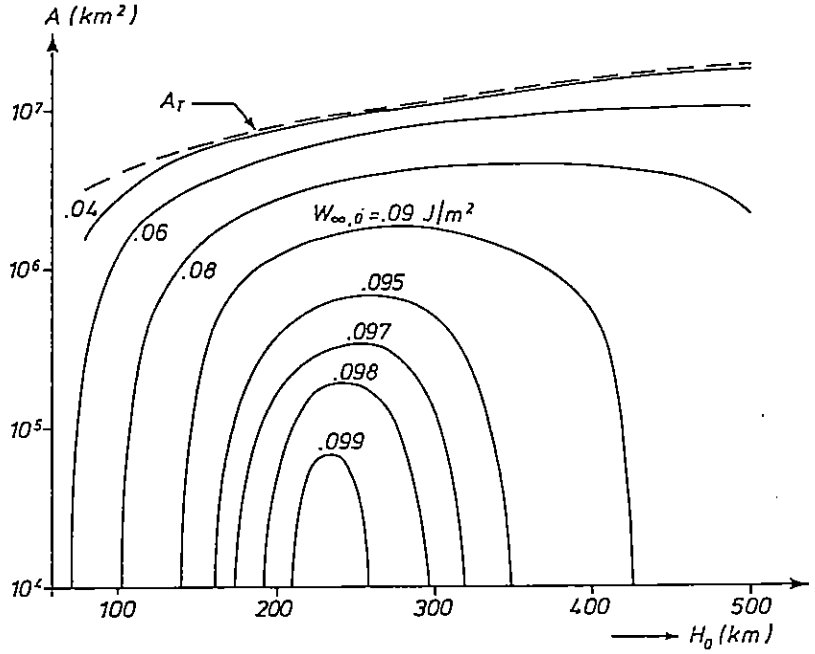

Fig. 3 Partial coverage area $A = A(W_\infty > W_{\infty,0})$ as a function of height of burst (A_T: total coverage area, $Y_\gamma = 10$ kt).

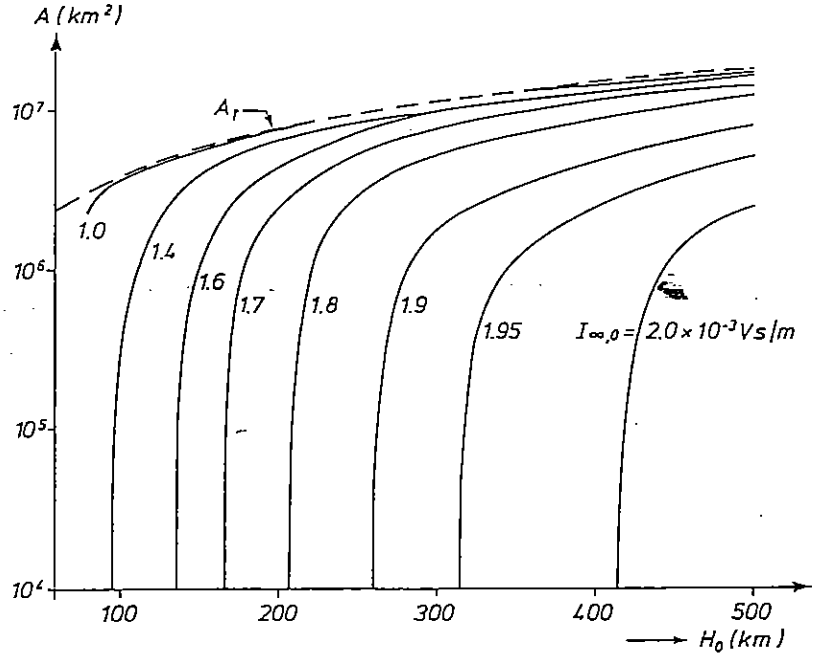

Fig. 4 Partial coverage area $A = A(I_\infty > I_{\infty,0})$ as a function of height of burst (A_T: total coverage area, $Y_\gamma = 10$ kt).

Table 1

Maximum and average values of Q_i for different heights of burst and a gamma yield of 10 kt

(Units: E_{pk} (kV / m), $\dot{E}_{pk}$ (kV / m / ns), W_∞ (mJ / m²), I_∞ (mVs / m))

H_o	$E_{pk,\,max}$	$\langle E_{pk} \rangle_{av}$	$\dot{E}_{pk,\,max}$	$\langle \dot{E}_{pk} \rangle_{av}$	$W_{\infty,\,max}$	$\langle W_\infty \rangle_{av}$	$I_{\infty,\,max}$	$\langle I_\infty \rangle_{av}$
80	59.5	31.8	42.0	16.4	64.0	40.9	1.26	1.06
100	63.0	36.5	37.0	13.8	77.4	51.1	1.43	1.22
150	62.6	38.5	29.1	9.7	94.3	64.8	1.65	1.42
200	59.0	37.5	23.0	7.3	98.8	69.3	1.77	1.53
250	55.0	35.0	17.9	5.67	99.2	71.0	1.89	1.64
300	51.2	32.7	14.6	4.64	97.8	70.5	1.94	1.68
400	44.5	28.3	10.0	3.35	91.7	67.0	1.99	1.72
500	38.8	24.5	7.4	2.56	84.4	62.4	2.00	1.75

The ratio of peak electric field at the horizon and the location where E_{pk} has its maximum varies from about 35 % at low heights of burst to 46 % for $H_o > 250$ km. There is a more distinct decrease of the peak rate of rise and a slower decrease of the energy fluence when approaching the horizon. The reason for the latter is a considerable increase of the pulse duration with increasing ground range.

Fig. 5 and Fig. 6 show normalized coverage areas $A\,(Q_i > Q_{io}) / A_T$ as a function of the gamma yield calculated for H_o = 100 km. The corresponding maximum and average values of Q_i are shown in Table 2.

As can be seen from these data the ratio $Q_i\,(R_T) / Q_{i,max}$ decreases remarkably for lower yields. At the same time the location of maximum peak electric field moves towards Ground Zero, as can be observed from Table 3.

The last two columns of Table 3 show energy fluence and impulse at the location R_{max} of maximum peak electric field. Comparing these numbers with the

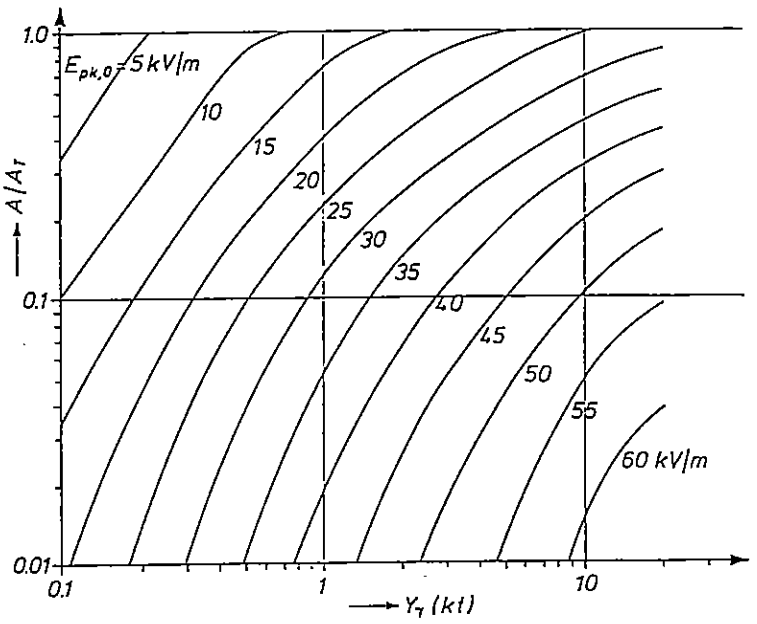

Fig. 5 Partial coverage area $A = A\,(E_{pk} > E_{pk,o})$ as a function of gamma yield Y_γ (A_T : total coverage area, HOB = 100 km).

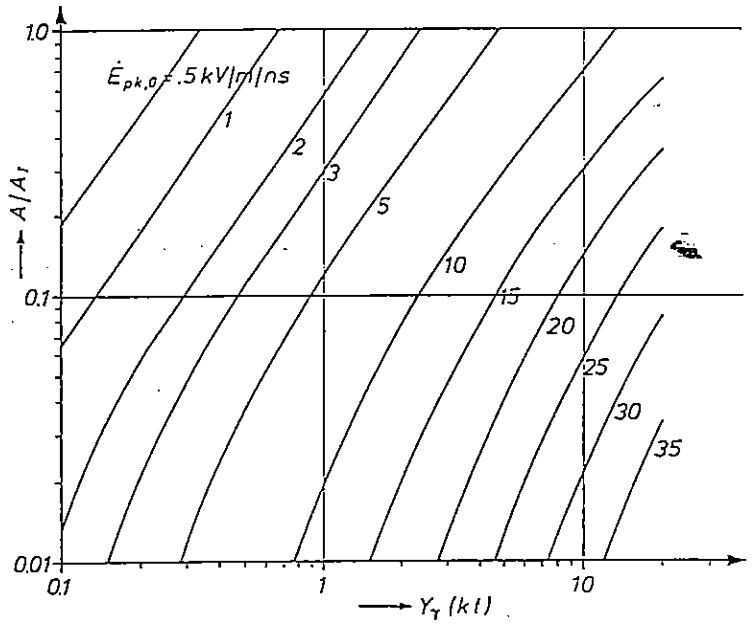

Fig. 6 Partial coverage area $A = A\,(\dot{E}_{pk} > \dot{E}_{pk,o})$ for as a function of gamma yield Y_γ (A_T : total coverage area, HOB = 100 km).

corresponding maximum values as represented in Table 2 gives an indication for the weak correlation of the respective distribution functions.

Table 2

Maximum and average values of Q_i for different yields and a height of burst of 100 km (units as in Table 1)

Y_γ (kt)	$E_{pk,\,max}$	$\langle E_{pk} \rangle_{av}$	$\dot{E}_{pk,\,max}$	$\langle \dot{E}_{pk} \rangle_{av}$	$W_{\infty,\,max}$	$\langle W_\infty \rangle_{av}$	$I_{\infty,\,max}$	$\langle I_\infty \rangle_{av}$
0.1	23.3	5.4	3.2	0.40	36.6	7.5	1.29	0.77
0.2	29.8	9.0	5.5	0.75				
0.5	38.7	15.4	10.1	1.7				
1	45.4	20.6	15.2	3.0	62.2	31.7	1.39	1.14
2	51.2	25.6	21.1	5.0				
5	57.9	31.9	29.7	9.3				
10	63.0	36.5	37.0	13.8	77.4	51.1	1.43	1.22
20	66.0	40.2	42.3	19.2				

Table 3

Maximum and at-the-horizon peak electric fields in units of kV/m for different gamma yields. R_{max} is the distance southward of GZ in units of H_o = 100 km where E_{pk} has a maximum (units as in Table 1).

Y_γ (kt)	R_{max}	$E_{pk,\,max}$	$E_{pk}(R_T)$	%	$W_\infty(R_{max})$	$I_\infty(R_{max})$
0.1	0.85	23.3	2.73	12	31	0.83
1	1.31	45.4	13.1	29	47	0.78
10	1.64	63.0	25.2	40	49	0.68
20	1.74	66.0	28.1	43	50	0.66

The cumulative probabilities of the normalized quantities $Q_i / Q_{i,max} \equiv f_i$ are summarized in Fig. 7 (for $H_o = 200$ km and $Y_\gamma = 10$ kt) and in Fig. 8 (for $H_o = 100$ km and $Y_\gamma = 1$ kt). A comparison of the two figures demonstrates again the stronger decrease of E_{pk} and dE_{pk}/dt when approaching the horizon for the lower yields. Respective probability density functions are presented in Figs 11 to 14 (see Section 3).

Fig. 9 shows the distribution of the elevation angle of the electric field vector with respect to the earth surface

$$\theta = \left| \arcsin \left(E_z / E \right) \right| \tag{12}$$

where E_z and E are the vertical component and the magnitude of the total electric field vector, respectively. Because the orientation of the electric field is approximately perpendicular to both the earth magnetic field and the line-of-sight vector from the observer location to the burst point, θ is nearly independent of the height of burst. The gamma yield shows also little influence.

For EMP interaction calculations the decomposition of the incident wave into vertically and horizontally polarized parts plays a more important role than θ because it takes also the elevation of the propagation vector (i.e. line-of-sight) with respect to the earth surface into account. Hence, the distribution functions of the vertical and horizontal degrees of polarization P_v and P_h are also plotted in Fig. 10. The dominance of horizontal polarization is quite evident. More detailed information on the polarization can be found in the references [4,5].

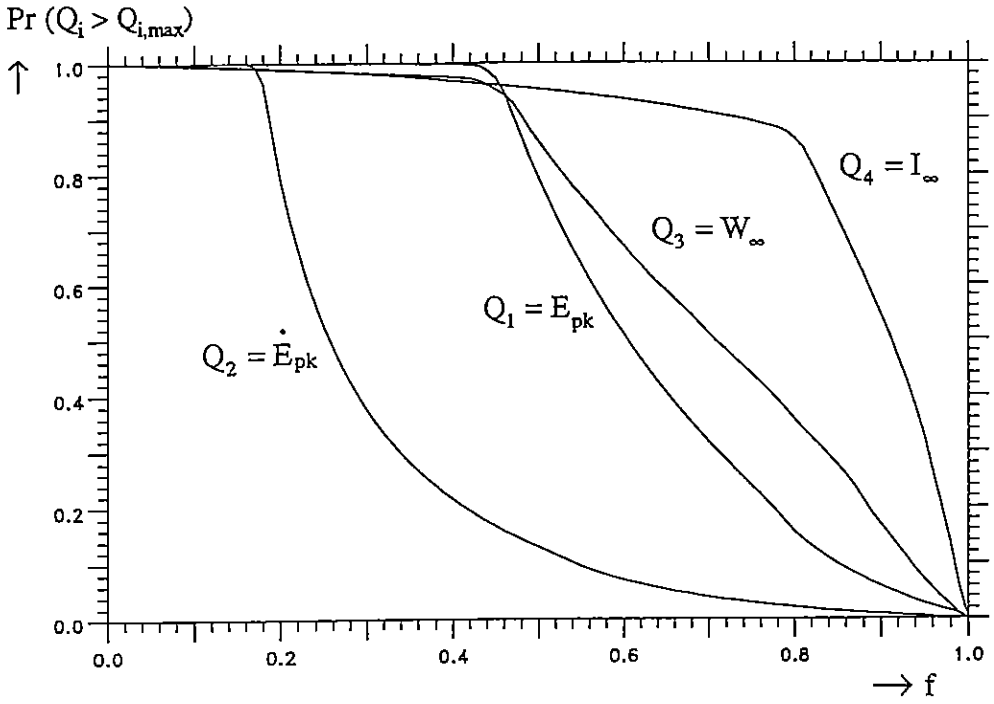

Fig.7 Cumulative probabilities Pr $\left(Q_i > f\, Q_{i,max}\right)$ *for* $H_O = 200$ *km and* $Y_\gamma = 10$ *kt.*

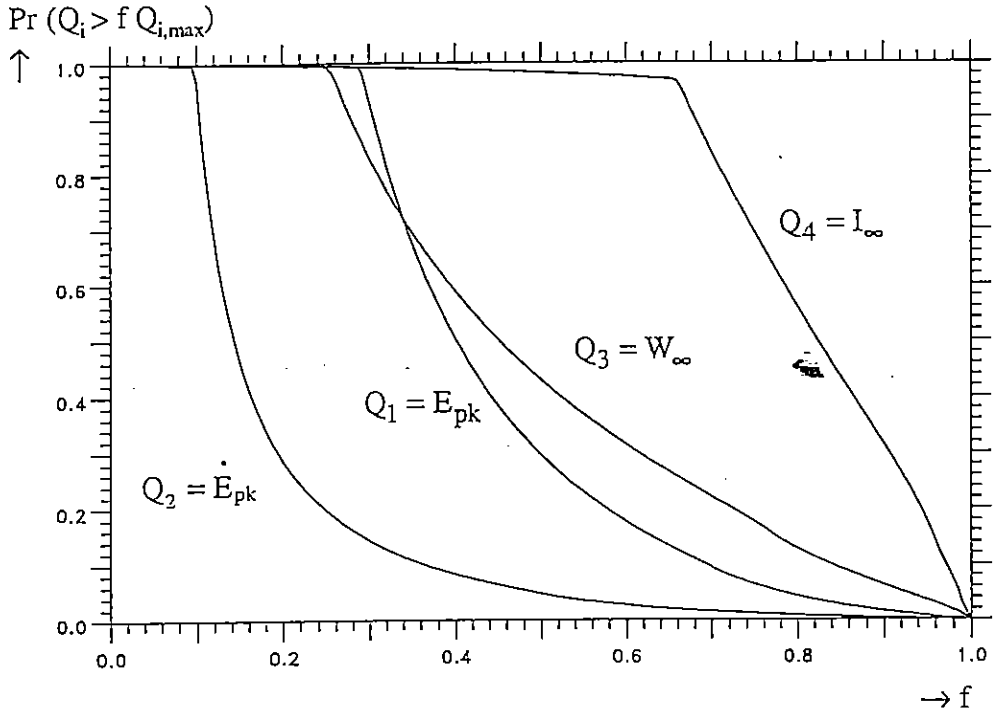

Fig. 8 Cumulative probabilities Pr $\left(Q_i > f\, Q_{i,max}\right)$ *for* $H_O = 100$ *km and* $Y_\gamma = 1$ *kt.*

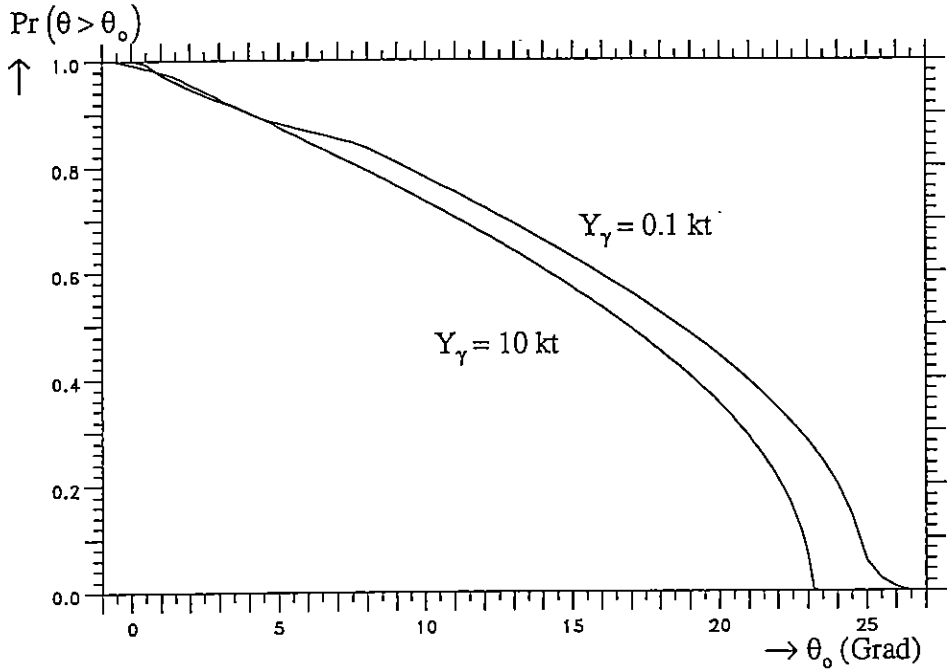

Fig. 9 Cumulative probabilities $Pr(\theta > \theta_o)$ of the elevation angle θ of the electric field vector with respect to the local horizontal plane.

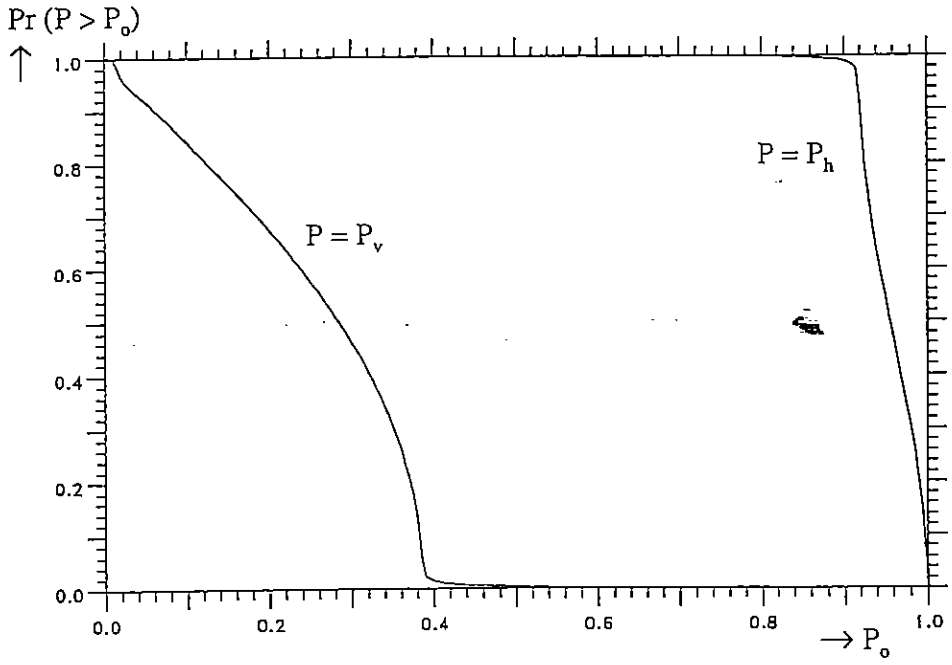

Fig. 10 Cumulative probabilities $Pr(P > P_o)$ of the polarization degrees P_h and P_v for horizontal and vertical polarization, respectively.

3. Bivariate Distributions

The Monte Carlo method is particularly well suited to calculate bi- or multivariate distribution functions, e.g.

$$\Pr\left(Q_i > Q_{i,o},\ Q_j > Q_{j,o}, \ldots.\right), \quad i \neq j \tag{13}$$

which, geometrically, is the intersection of the coverage areas for which $Q_i > Q_{i,o}$ and $Q_j > Q_{j,o}$, respectively,

$$A\left(Q_i > Q_{i,o}, Q_j > Q_{j,o}\right) = A\left(Q_i > Q_{i,o}\right) \cap A\left(Q_j > Q_{j,o}\right) \qquad i \neq j. \tag{14}$$

Table 4 is an example of a correlation matrix between E_{pk} and W_∞ with $H_o = 200$ km and $Y_\gamma = 10$ kt. Table 5 represents the correlation matrix between E_{pk} and I_∞.

Table 4

Fractions of the total coverage area for which
$E_{pk} > f_1 E_{pk,max}$ *and* $W_\infty > f_3 W_{\infty,max}$

	$f_1 = E_{pk} / E_{pk,max}$						
f_3	.00	.30	.50	.60	.70	.80	.90
.00	1.0000	0.9977	0.7695	0.4928	0.3023	0.1431	0.0512
.10	0.9937	0.9937	0.7691	0.4928	0.3023	0.1431	0.0512
.20	0.9877	0.9877	0.7636	0.4905	0.3019	0.1431	0.0512
.30	0.9811	0.9811	0.7570	0.4840	0.2988	0.1424	0.0512
.40	0.9732	0.9732	0.7490	0.4761	0.2920	0.1394	0.0509
.60	0.6679	0.6679	0.6679	0.4541	0.2700	0.1253	0.0433
.70	0.5092	0.5092	0.5092	0.4382	0.2541	0.1139	0.0367
.80	0.3565	0.3565	0.3565	0.3565	0.2298	0.0953	0.0250
.85	0.2749	0.2749	0.2749	0.2749	0.2118	0.0842	0.0185
.90	0.1686	0.1686	0.1686	0.1686	0.1643	0.0687	0.0089
.95	0.0715	0.0715	0.0715	0.0715	0.0715	0.0366	0.0000
.98	0.0247	0.0247	0.0247	0.0247	0.0247	0.0158	0.0000
.99	0.0084	0.0084	0.0084	0.00840.	0.0084	0.0048	0.0000

Table 5

Fraction of the total coverage areas for which
$E_{pk} > f_1 \; E_{pk,max}$ *and* $I_{\infty} > f_4 \; I_{\infty,max}$

	$f_1 = E_{pk} \; / \; E_{pk,\,max}$						
f_4	.00	.30	.50	.60	.70	.80	.90
.00	0.9886	0.9956	0.7695	0.4928	0.3023	0.1336	0.0512
.10	1.0000	0.9977	0.7695	0.4928	0.3023	0.1431	0.0512
.20	0.9956	0.9886	0.7644	0.4906	0.3016	0.1431	0.0512
.30	0.9793	0.9793	0.7552	0.4822	0.2965	0.1431	0.0512
.40	0.9669	0.9669	0.7428	0.4698	0.2858	0.1406	0.0510
.50	0.9519	0.9519	0.7278	0.4548	0.2708	0.1230	0.0469
.60	0.9328	0.9328	0.7087	0.4357	0.2517	0.1079	0.0398
.70	0.9085	0.9085	0.6844	0.4114	0.2273	0.0879	0.0292
.80	0.8609	0.8609	0.6488	0.3758	0.1918	0.0589	0.0160
.85	0.7154	0.7154	0.6235	0.3505	0.1664	0.0396	0.0000
.90	0.5416	0.5416	0.5416	0.3136	0.1296	0.0139	0.0000
.95	0.3255	0.3255	0.3255	0.2516	0.0683	0.0000	0.0000
.98	0.1296	0.1296	0.1296	0.1296	0.0230	0.0000	0.0000
.99	0.0550	0.0550	0.0550	0.0550	0.0088	0.0000	0.0000

Bivariate distribution functions can be useful in discussing a systematic approach to reduce worst case threat data in conjunction with EMP protection of lower value targets.

As shown in [2] a worst case set of EMP threat parameters $\{Q_{max}\}$ refers to different heights of bursts and observer locations. Hence, a ground observer at a fixed position can never experience the full set of worst case parameters in a single burst.

A deliberate reduction of $E_{pk,\,max}$ by 20 % (i.e. $f_1 = 0.8$) would result in ignoring or cutting out a kidney-shaped area southward of Ground Zero amounting to 14.4 % of the whole coverage area A_T. As can also be seen from Table 4, the reduction of $E_{pk,\,max}$ has negligible influence on $W_{\infty,\,max}$ because the location of maximum energy fluence is just outside the cut off area. This also applies for I_∞.

The following Figs 12 to 14 visualize the cut off effect on the probability density functions

$$g_i(f) = \frac{d}{df} \Pr\left(Q_i > f\, Q_{i,\,max}\right), \qquad i = 2,3,4 \tag{15}$$

for the cut off levels $f_1 = 0.6$ to 1.0. The probability density function g_1 (f) for $Q_1 = E_{pk}$ is given in Fig. 11 for completeness.

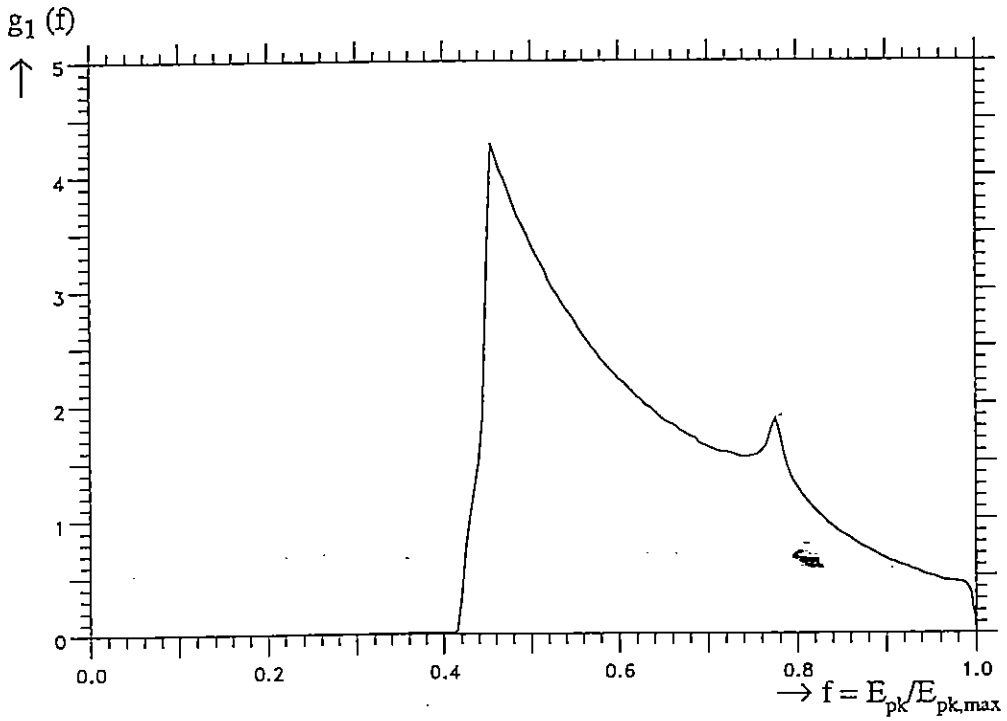

Fig. 11 Probability density function g_1 (f) of the peak electric field magnitude (H_o = 200 km, Y_γ = 10 kt).

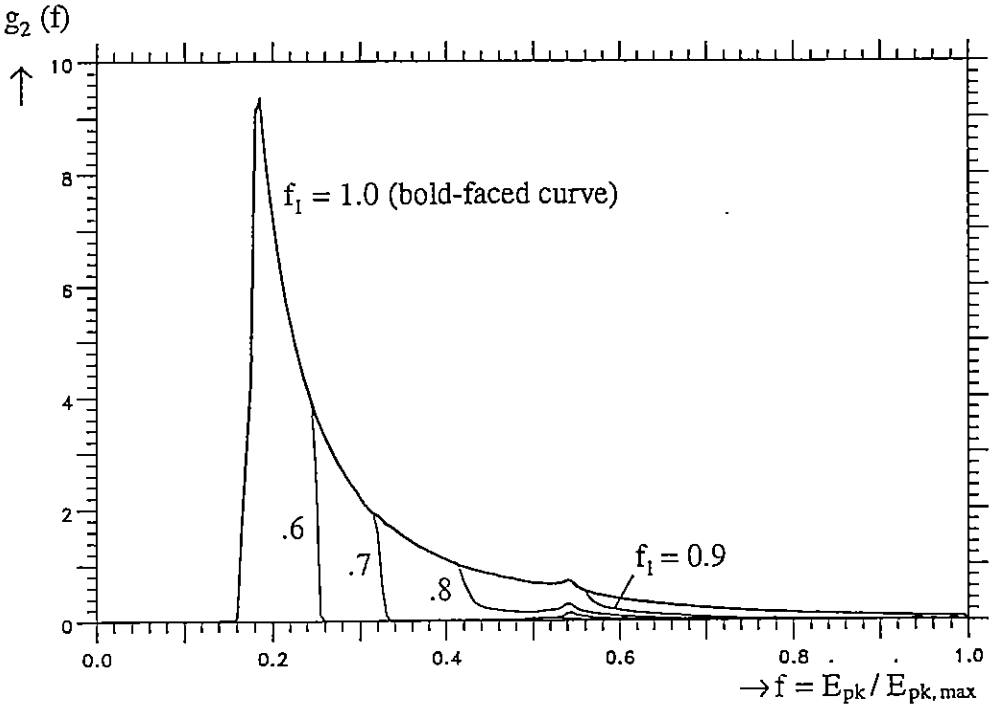

Fig. 12 Probability density functions g_2 (f) of the peak rate of rise $\dot{E}_{pk}$ for various reduction levels f_1 of the peak electric field magnitude.

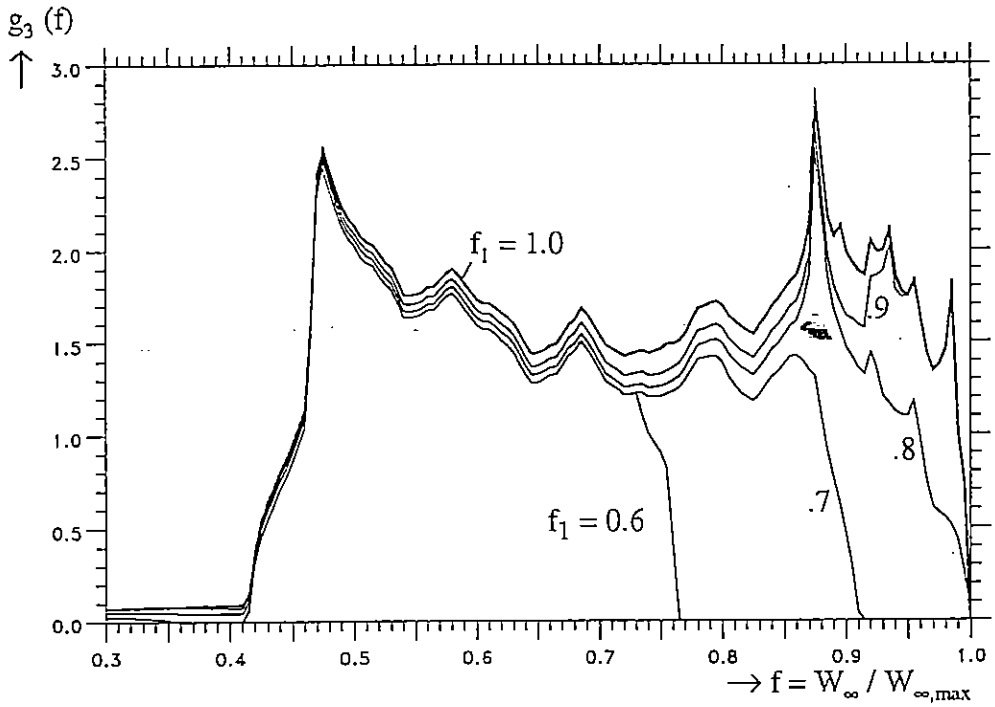

Fig. 13 Probability density functions g_3 (f) of the energy fluence W_∞ for various reduction levels f_1 of the peak electric field magnitude.

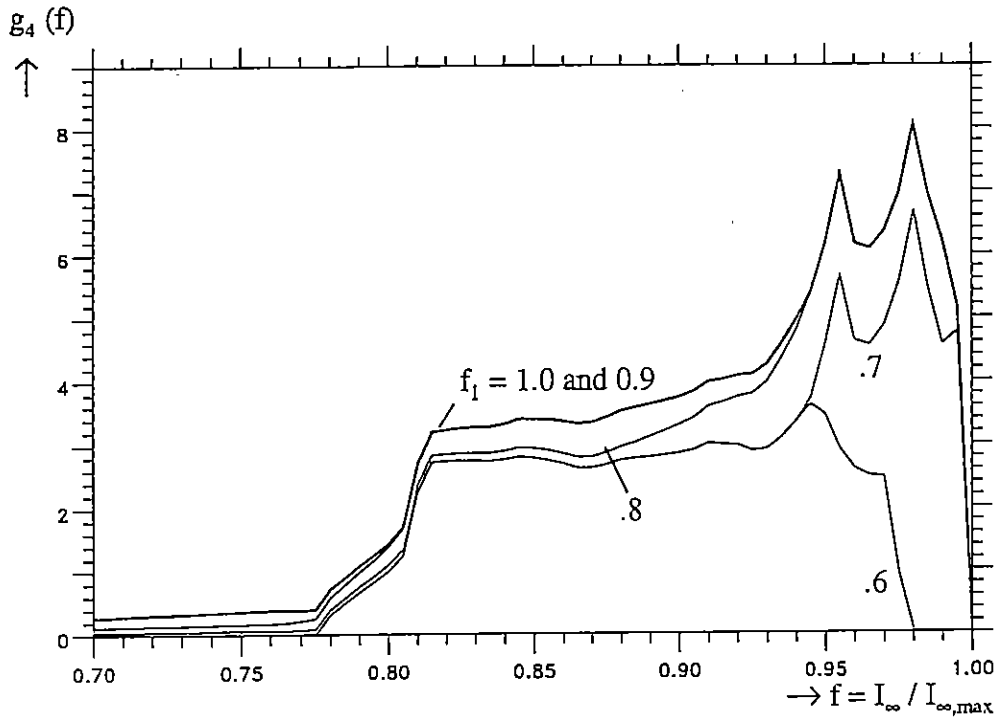

Fig. 14 Probability density functions g_4 (f) of the impulse function I_∞ for various reduction levels f_1 of the peak electric field magnitude.

Table 6 summarizes consistent sets of reduced worst case parameters under different reduction conditions.

Table 6

f_1	$Pr\left(E_{pk} > f_1 E_{pk,max}\right)$	$E_{pk,max}$	$\dot{E}_{pk,max}$	$W_{\infty,max}$	$I_{\infty,max}$
1.0	0	59.8	23.0	98.8	1.77
0.9	0.052	53.8	22.9	98.8	1.77
0.8	0.144	47.8	20.8	98.8	1.77
0.7	0.303	41.9	18.2	89.9	1.76

Table 7 offers QEXP fits

$$E(t) = \frac{k\,E_{pk}}{e^{-\alpha t} + e^{\beta t}} \qquad (16)$$

for the data given in Table 6.

Table 7

QEXP fit parameters

f_1	k	$\alpha\,(s^{-1})$	$\beta\,(s^{-1})$	$W_\infty^{QEXP}\,(mJ/m^2)$
1.0	1.13	1.40×10^9	3.82×10^8	151
0.9	1.11	1.57×10^9	3.37×10^8	134
0.8	1.09	1.62×10^9	2.96×10^8	119
0.7	1.08	1.63×10^9	2.58×10^8	103

Since the four $Q_{i,\,max}$ cannot be fitted by Eq. (16) simultaneously [2], the fit was performed to match the maximum values of $Q_4 = I_{\infty,\,max}$ (being identical with the low frequency limit < 2 MHz), $Q_2 = (dE/dt)_{pk,\,max}$ (determining the behavior at frequencies > 200 MHz) amd $Q_1 = E_{pk,\,max}$.

For intermediate frequencies (20 MHz to 200 MHz), the envelope of the amplitude spectra for all different observer positions (which can be defined as the worst case threat) is governed by the EXEMP calculated pulses in the vicinity of the location of maximum peak electric field (R ≈ 1.4 southward of GZ). For these intermediate frequencies, the QEXP fit for the unreduced case $(f_1 = 1.0)$ is in good agreement with the envelope. Because a reduction of E_{pk} by 20 % ($f_1 = 0.8$) does not imply substantial changes of $(dE/dt)_{pk}$ and I_∞, the frequency spectrum will therefore be reduced only in the range 10 MHz to 200 MHz by no more than 30 % with respect to the reference case $f_1 = 1.0$.

In general, the QEXP fitting procedure overestimates W_∞. The energy fluences calculated by means of Eq. (16) are given in the last column of Table 7.

4. Concluding Remarks

The probabilistic considerations performed in Section 3 were restricted to a given height of burst (i.e. 200 km). A complete picture of the HEMP environment would have to include variations of height of burst, yield, Ground Zero and perhaps other parameters. As shown in [2] and Figs 1 and 2, Q_1 and Q_2 acquire their absolute maxima for HOBs below 200 km, whereas Q_4 continuously increases from low HOBs to 500 km (Fig. 4). Because, however, an HEMP would have to be considered as a singular event for which all scenario and weapon oriented data are not predictable, the latter should be investigated only parametrically. The assumption of any distribution functions does not seem to be very meaningful.

References

1. K.-D. Leuthäuser, A Complete EMP Environment Generated by High-Altitude Nuclear Bursts, TN 363, 1992
2. K.-D. Leuthäuser, A Complete EMP Environment Generated by High-Altitude Nuclear Bursts: Data and Standardization, TN 364, 1994
3. C.E. Baum: Some Considerations Concerning Analytic EMP Criteria Wave-Forms, TN 285, 1976
4. W.A. Radasky and M.A. Messier: HEMP Environment Polarization and Incidence Issues for Coupling Problems, EUROEM Conference, Bordeaux, France, June 1994
5. K.-D. Leuthäuser and S. Scheid: On the Polarization of the High-Altitude Electromagnetic Pulse (in German), INT Report No. 157, January 1995